Electronic Supplementary Information (ESI) for

Enhanced osteoblast differentiation and osseointegration of a bio-inspired HA nanorods patterned pores-sealed MgO bilayer coating on magnesium

Bo Li [1], Yong Han [1]*, Mei Li [1, 2]

1. State Key Laboratory for Mechanical Behavior of Materials, Xi'an Jiaotong University, Xi'an 710049, China.

2. Hospital of Orthopedics, Guangzhou General Hospital of Guangzhou Military Command, Guangzhou 510010, China.

* Corresponding author: yonghan@mail.xjtu.edu.cn (Y. Han).

1. Additional experimental method

1.1 Evaluation of apatite-inducing ability of HT24h coating

The apatite-inducing ability of HT24h coating was examined in simulated body fluid (SBF). The SBF solution was prepared by dissolving reagent-grade chemicals (NaCl, $NaHCO_3$, KCl, $K_2HPO_4 \cdot 3H_2O$, $MgCl_2 \cdot 6H_2O$, $CaCl_2$ and Na_2SO_4) in distilled water, and buffering at pH 7.4 with tris-hydroxymethyl-aminomethane and HCl at 36.5 ℃. The ions concentrations (mM) of the solution are 142 Na^+, 5 K^+, 1.5 Mg^{2+}, 2.5 Ca^{2+}, 147.8 Cl^-, 4.2 HCO_3^-, 1 HPO_4^{2-} and 0.5 SO_4^{2-}, nearly equal to those of human blood plasma. Each HT24h-coated Mg disc was immersed in a plastic vial containing 50 mL of SBF and was kept under static condition inside a biological thermostat at 36.5 ℃ for 12 h. At the end of immersion period, the HT24h-coated Mg discs were removed from SBF, washed with distilled water and then air dried. The surface morphologies of HT24h-coated Mg discs after immersion were examined by field-emission scanning electron microscopy (FE-SEM; JEOL JSM-6700F, Japan).

2. Additional results

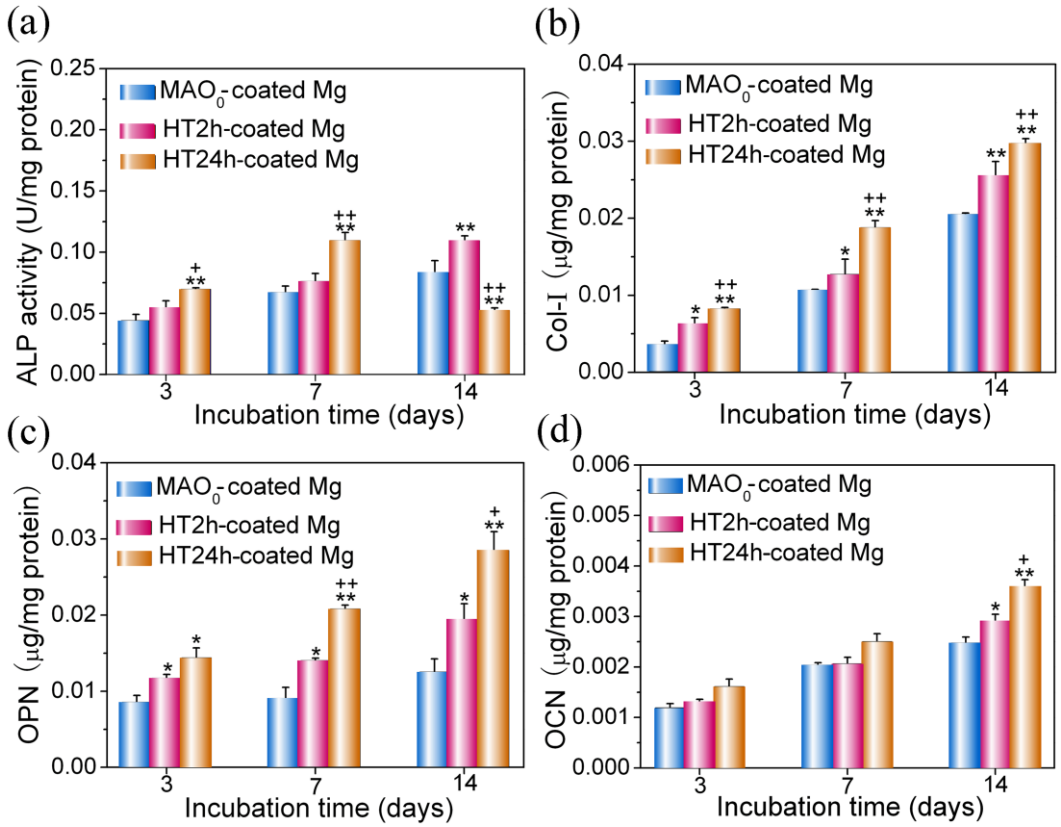

Fig. S1 (a) ALP activity as well as contents of (b) Col-I, (c) OPN, and (d) OCN proteins in osteoblasts cultured on MAO_0-, HT2h- and HT24h-coated Mg for 3, 7, and 14 days. Data are presented as the mean ± SD, n = 4, (*) $p < 0.05$ and (**) $p < 0.01$ compared with MAO_0-coated Mg, (+) $p < 0.05$ and (++) $p < 0.01$ compared with HT2h-coated Mg.

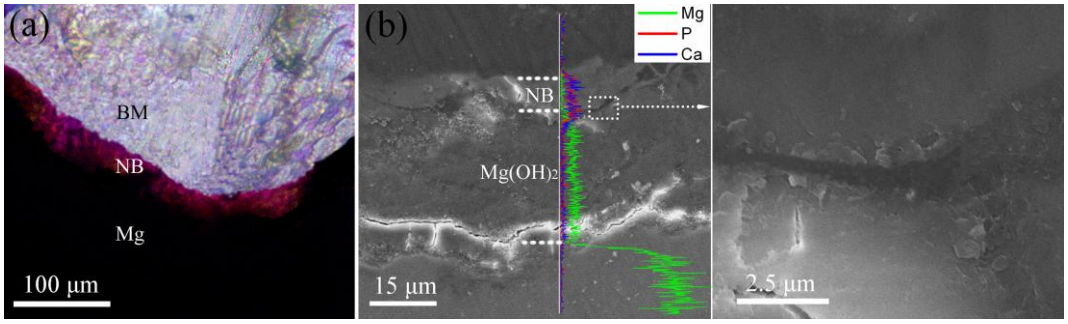

Fig. S2 (a) Histological analysis performed on the cross-section of bare Mg pillar implanted in rabbit femur for 8 weeks; NB: new bone, BM: bone marrow. (b) Cross-sectional FE-SEM morphology at the interface of new bone and the bare pillar together with the magnified image of the interface, showing an obvious gap.

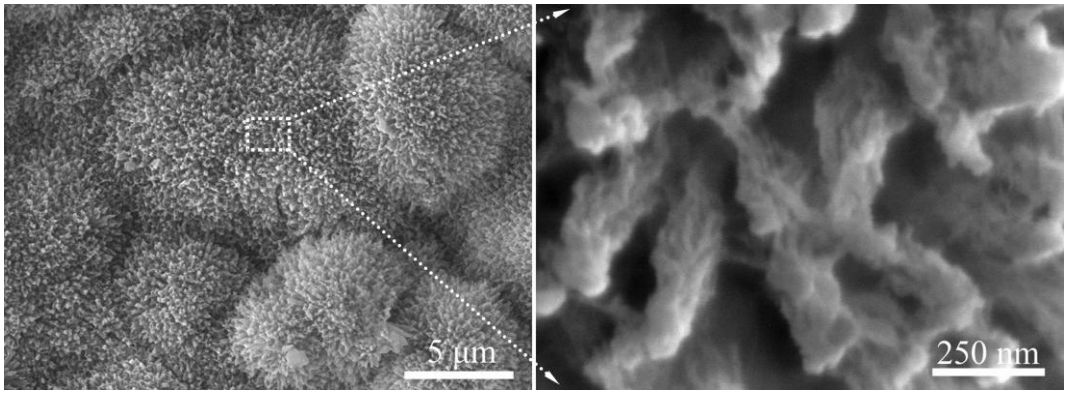

Fig. S3 Low-magnification FE-SEM surface morphology of the HT24h-coated Mg disc immersed in SBF for 12 h together with the magnified image of the square-dotted marked area.

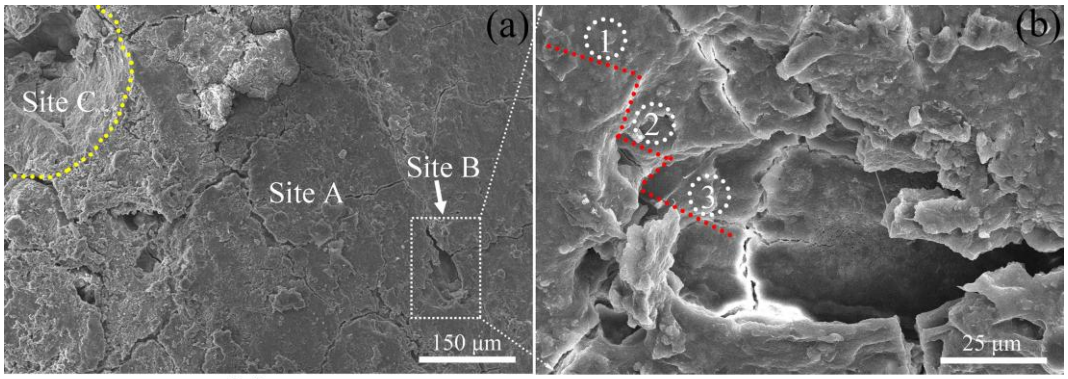

(c)

Elements	C	O	Na	Mg	P	Ca
Point 1	25.54	31.83	01.14	32.20	04.21	05.07
Point 2	24.97	34.38	00.76	36.17	02.00	01.71
Point 3	17.60	40.43	00.48	40.52	00.29	00.68
Point φ	11.94	35.13	-	36.80	07.60	08.52

Fig. S4 (a) FE-SEM surface image of the pushed-out disrupted surface on HT2h-coated Mg pillar implanted in rabbit femur for 8 weeks, and (b) magnified image of site B in (a). (c) listing the elemental compositions (at.%) detected at the points 1~3 marked in the above-mentioned images, together with that detected at point φ on HT2h coating shown in Fig. 1.

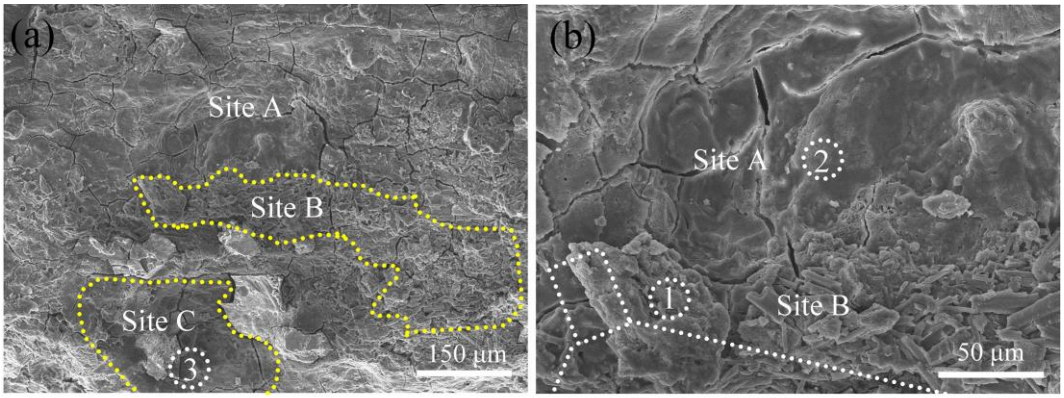

(d)

Elements	C	O	Na	Mg	P	Ca
Point 1	27.35	34.05	03.41	31.08	02.23	01.89
Point 2	16.63	41.83	00.95	40.10	00.33	00.17
Point 3	14.82	42.22	00.60	41.85	00.36	00.14
Point δ	10.59	35.96	-	38.01	08.70	06.73

Fig. S5 (a) FE-SEM surface image of the pushed-out disrupted surface on MAO_0-coated Mg pillar implanted in rabbit femur for 8 weeks, (b) magnified image of site B in (a), (c) magnified image of the dotted-square marked area in (b). (d) listing the elemental compositions (at.%) detected at the points 1~3 marked in the above-mentioned images, together with that detected at point δ on MAO_0 coating shown in Fig. 1.

For HT2h-coated pillar, three kinds of failure modes appeared on the disrupted surface, as shown in Fig. S4a. One is within the coating but near its surface (site A in Fig. S4a), as verified by the detected Ca and P but slightly decreased contents of the elements at point 1 than those at point φ. The other appears at HT2h coating/Mg interface (site B in Fig. S4a and magnified b), as indentified by higher contents of Mg and O but absence of Ca and P at point 3 compared to points 1 and 2. The last is at corrosion pits (site C in Fig. S4a), as evidenced by the deep pit-shaped feature. The

area percentage of the failure modes (Fig. 8f) indicates that the disruption within coating but near its surface is a predominant failure mode for HT2h-coated Mg pillar.

Moving to MAO_0-coated pillar, three kinds of failure modes could be observed on the disrupted surface from Fig. S5: (1) failure at MAO_0 coating/Mg interface (site A in Fig. S5a and magnified b), as identified by the large scale of plain morphology and higher contents of Mg and O but absence of Ca and P at point 2 compared to point 1; (2) failure within the coating but far from its surface (site B in Fig. S5a and magnified b), as identified by the detected Ca and P but significantly decreased contents of the elements at point 1 than those at point δ; (3) failure at corrosion pits (site C in Fig. S5a), as identified by the deep pit-shaped feature and higher contents of Mg and O but absence of Ca and P detected at point 3 compared to point 1. Of which the disruption at the coating/Mg interface is a predominant failure mode.